RSC Advances

ROYAL SOCIETY OF CHEMISTRY

www.rsc.org/advances

Effectiveness of carbon nanotube/cobalt ferrite nanocomposites for the adsorption of rhodamine B from aqueous solutions

Oluwaseun A. Oyetade, Vincent O. Nyamori,* Bice S. Martincigh and Sreekantha B. Jonnalagadda

School of Chemistry and Physics, University of KwaZulu-Natal, Westville Campus, Private Bag X54001, Durban 4000, South Africa

*Corresponding author: Tel: +27 31 260 8256; Fax: +27 31 2603091; E-mail address: nyamori@ukzn.ac.za (V.O. Nyamori)

Abstract

The efficiency of adsorption of rhodamine B (RhB) from aqueous solution was investigated through a series of batch experiments by using cobalt ferrite nanoparticles ($CoFe_2O_4$), acid-functionalized multiwalled carbon nanotubes (MWCNT-COOH) and carbon nanotube-cobalt ferrite nanocomposites. The adsorption capacity was evaluated as a function of pH, contact time, adsorbent dose, dye concentration and temperature. The effect of increasing the percentage of MWCNT-COOH in the nanocomposites was also studied. The adsorption capacity was lowest in $CoFe_2O_4$ (5.165 mg g^{-1}) and highest with MWCNT-COOH (42.68 mg g^{-1}). For the nanocomposites, the adsorption capacity was enhanced with an increase in the amount of MWCNT-COOH. The optimum pH for adsorption was observed at 7 at which equilibrium was reached after 360 min. The kinetics of adsorption was fitted to the pseudo-first order, pseudo-second order, Elovich and intraparticle diffusion models. The results showed that the pseudo-second order model best described the data as reflected in the lowest value for the sum of squared residuals. Among the various adsorption isotherms tested, the Langmuir isotherm provided the best fit to the equilibrium data. The thermodynamic parameters, $\Delta H°$, $\Delta S°$ and $\Delta G°$, were obtained over a temperature range of 20-45 °C. Adsorption was spontaneous, endothermic and entropy-driven, except for one of the doped nanocomposites for which adsorption was exothermic. A good desorption of RhB from the loaded adsorbents was obtained by using either acetone or ethanol with a desorption efficiency in the range of 62-95%.

Keywords: Multiwalled carbon nanotubes, cobalt ferrite nanoparticles, nanocomposites, adsorption, wastewater, rhodamine B

1. Introduction

Treatment of wastewater generated from textile manufacturing, printing and dyeing is a major environmental problem due to the presence of dissolved dye materials. Rhodamine B (RhB) is a basic red cationic dye, usually used for commercial and industrial applications. The indiscriminate discharge of RhB-contaminated effluents into aqueous media introduces man, aquatic life and the environment to potentially harmful effects, ranging from minor irritations to major diseases.[1-3] Water, which makes up about 70 % of the earth's surface, is a principal recipient of the discharge of organic and inorganic pollutants. Since freshwater is a limited resource, the remediation of wastewater before its disposal is of major importance. Several techniques, such as coagulation,[4,5] chemical oxidation,[6-8] photochemical,[9,10] membrane separation and ion exchange,[11] irradiation,[12] decolourization by white fungi,[13] ozonation,[14,15] electrochemical destruction[16,17] and aerobic/anaerobic microbial degradation,[2,7] have been proposed for dye remediation in wastewater. In spite of the availability of these methods, steep challenges, such as sludge generation, high usage of energy, generation of dissolved oxygen, longer retention time,[2] release of aromatic compounds, formation of by-products, high operation costs and operation difficulty, are characteristic of these processes.[1]

Adsorption has been considered ideal for the removal of pollutants from the environment because it is economically feasible and time-saving with easy operation. Also, adsorbents exhibit high pollutant removal efficiency and are easily regenerated/reused.[18] Due to these facts, many studies have been tailored towards the removal of pollutants with this technique. Materials such as activated carbon,[19] bagasse,[20] peanut hull,[21] charcoal,[3] hydrogels,[22] clay,[23] organomontmorillonites,[24] fly ash,[25] red mud,[26] kaolinite,[27] leaves,[28] dimethyl terephthalate,[29]

resin,[30] chestnut[31] and fruit waste[32,33] have been used for the removal of dyes from wastewater. However, limitations such as cost, loss of adsorption efficiency after regeneration, slow sorption and inconveniences encountered during separation are recognizable facts.

For these reasons, magnetic separation has been used as a preferred method for the removal of pollutants because it is easy, suitable for bulk solutions in heterogeneous systems and serves as a fast method of separation under external magnetic fields. Magnetic nanoparticles are considered potential adsorbents for aqueous pollutants due to the high surface area[34] possessed by these materials. Several nanoparticles, such as nickel ferrites,[34] maghemite,[35] and magnetite,[36] among others, have been proposed for effective removal of dyes in aqueous solution.

Since the discovery of carbon nanotubes (CNTs),[37] they have emerged as an adsorbent of interest for the removal of organic and/or inorganic pollutants from the environment.[38,39] CNTs possess tubular nanostructures with unique mechanical, physical, chemical and electrical properties,[38] and possess large surface areas in addition to their layered structures.[40] Due to their hydrophobicity, they are usually oxidized with acids to improve dispersion in water. Modification of CNTs to attach acidic groups has been attempted through both chemical and physical methods.[41] Chemical functionalization with acids causes shortening and thinning of tubes, and introduces polar functional groups such as -COOH and -OH on the tips or side-walls of CNTs.[42] This process helps in improving electrostatic interaction for removal of organic and/or inorganic pollutants onto CNTs. The use of CNTs as adsorbents

for removal of pollutants such as heavy metals,[18,43] polychlorinated biphenyls (PCBs)[44] and trihalomethane,[39] among many others, has also been explored.

Magnetic nanocomposites often allow easy separation of adsorbents from an aqueous phase by means of an external magnetic field.[34] This process overcomes the limitation of separation often encountered when using CNTs.

In this study, we investigated the ability of cobalt ferrite nanoparticles ($CoFe_2O_4$) and functionalized multi-walled carbon nanotubes (MWCNT-COOH) to adsorb a representative dye, RhB, from aqueous solution. This particular dye was chosen for adsorption due to its toxic nature and wide use in industry, and the fact that its behaviour is similar to that of other dyes in its class. In addition, nanocomposites containing varying ratios of MWCNT-COOH and $CoFe_2O_4$ were synthesized and tested for RhB removal. The effect of increasing percentages of MWCNT-COOH in the nanocomposites was studied to determine the effect on the removal efficiency and to understand the processes/interactions involved in dye removal. To the best of our knowledge, no previous study has shown the effect of increasing concentrations of CNTs on $CoFe_2O_4$ for the removal of anthropogenic dyes. Batch adsorption processes involving the effect of pH, adsorbent dose, contact time, initial dye concentration and temperature were investigated to determine the optimum conditions necessary for RhB removal from aqueous solution. Studies on desorption of the dye were also performed to assess the durability, reusability and regeneration of the adsorbents.

2. Experimental

2.1. *Chemicals*

Pristine multiwalled carbon nanotubes (MWCNTs) (purity > 95 wt %) synthesized by chemical vapour deposition (CVD) were purchased from Cheap Tubes Inc. (Brattleboro, USA). The length of the MWCNTs ranged from 10 to 20 μm, with an average length of 17 μm. Their outer diameters fell between 30 to 50 nm, with an average outer diameter of 39 nm. Nitric (55 %), sulfuric (98 %) and hydrochloric (32 %) acids were purchased from CC Imelmann Ltd (Robertsham, South Africa). Rhodamine B was purchased from Coleman & Bell Co. (Norwood, USA) while $Fe(NO_3)_3.9H_2O$, NaOH, and $Co(NO_3)_2.6H_2O$ were purchased from Merck Chemicals Ltd (Gauteng, South Africa).

2.2. *Preparation of cobalt ferrite nanoparticles*

Cobalt ferrite nanoparticles were prepared by the co-precipitation method as reported by Maaz *et al*.[45] Solutions of 2 mol dm^{-3} $Fe(NO_3)_3.9H_2O$ and 1 mol dm^{-3} $Co(NO_3)_2.6H_2O$ were prepared, and 25 cm^3 of each solution were mixed and stirred under an inert atmosphere of nitrogen for 30 min. The pH of the resulting solution was then adjusted by the addition of 6 mol dm^{-3} NaOH to attain the desired pH range of 10–13. The mixture was stirred further for another 1 h under inert conditions. The resulting solid was filtered, and washed first with ethanol, and then with deionised water until a neutral pH was obtained.

2.3. Preparation of functionalized multi-walled carbon nanotubes

Pristine MWCNTs (1.5 g) were placed in a round-bottomed flask to which 100 cm^3 of concentrated hydrochloric acid (32 %) was added to remove metallic impurities from the tubes by dissolution. The suspension was stirred for 2 h; the tubes were filtered and washed with deionised water until a neutral pH was obtained. The MWCNTs were dried in a vacuum

oven at 80 °C overnight. The purified MWCNTs were functionalized by using a mixture of concentrated sulfuric and nitric acids in a volume ratio of 1:3 and refluxed at 80 °C for 12 h. The resulting solution was diluted with deionised water, filtered and the tubes washed with deionised water until a neutral pH was obtained.[46]

2.4. Preparation of composite samples (MWCNT-COOH-$CoFe_2O_4$)

MWCNT-COOH (1.5 g) were placed in 100 cm^3 of deionised water and stirred under an inert atmosphere of nitrogen for 30 min. Solutions of 2 mol dm^{-3} $Fe(NO_3)_3.9H_2O$ and 1 mol dm^{-3} $Co(NO_3)_2.6H_2O$ were prepared and an aliquot of 25 cm^3 of each solution was added to the CNT suspension. The mixture was continuously stirred at room temperature for 1 h. The suspension was then conditioned to a pH of 10 with the addition of 6 mol dm^{-3} NaOH solution, and allowed to stir at room temperature for another hour. The mixture was filtered, the solid washed with ethanol and subsequently with deionised water until a neutral pH was obtained.[45] The samples were dried at 80 °C in a vacuum oven overnight. Nanocomposites of varying percentages were prepared and labelled as MWCNT-$CoFe_2O_4$-29 %, MWCNT-$CoFe_2O_4$-50 % and MWCNT-$CoFe_2O_4$-75 %. Details of the compositions and sample identification are shown in Table 1.

[Insert Table 1]

2.5. Characterization of adsorbents

The specific surface area of the CNTs was determined with nitrogen as the flow gas by means of a Micromeritics Tristar II 3020 surface area and porosity analyser. Data were captured and analysed by using Tristar II 3020 version 2 software. Characterization of synthesized materials was done with a transmission electron microscope (TEM) (JEOL, TEM 1010) and a

high resolution transmission electron microscope (HRTEM) (JEOL, TEM 2100) to visualize the morphology, and to determine the shape and mean particle size. Images were captured by means of a Megaview 3 camera and analysed on iTEM software. Gatan digital micrograph software was used in analysing images obtained from HRTEM. Fourier transform infrared (FTIR) spectrometry (Perkin Elmer Spectrum RX 1 spectrometer) was used to characterize the surface functionalities on adsorbents by incorporating the materials in a KBr disc. Raman spectroscopy (DeltaNu Advantage 532^{TM}) measurements were performed to provide information on the purity and crystallinity of adsorbents.

2.5.1. Determination of point of zero charge (pH_{PZC})

Aliquots of 50 cm^3 of 0.01 mol dm^{-3} NaCl solutions were measured into bottles and adjusted with the addition of appropriate amounts of 0.1 mol dm^{-3} HCl or NaOH to obtain an initial pH in the range of 1-10. A mass of 100 mg of adsorbent was added into each bottle and the suspension left to equilibrate on an orbital shaker for 48 h. The solutions were filtered and the final pH of the filtrates determined. A plot of $pH_{initial} - pH_{final}$ against $pH_{initial}$ was obtained and the point of intersection of the curves gave the pH_{PZC} of the adsorbent.[31]

2.6. Adsorbate preparation

The dye (RhB) used in this study was of analytical grade and used without further purification. A calibration curve was obtained from dye solutions ranging from 1 to 7 mg dm^{-3} at a wavelength of maximum absorption (λ_{max}) of 554 nm by means of a UV-vis-NIR spectrophotometer (Shimadzu, UV-3600). The concentration of RhB in samples was determined by using the calibration curve prepared. A stock solution of RhB was prepared

by accurately weighing 1 g of the pure powder to make a solution containing 1 g dm^{-3} RhB in deionised water.

2.7. Batch adsorption procedure

Freshly prepared working solutions of RhB were prepared from the stock solution to obtain the required concentrations. The pH values of solutions were adjusted by adding an appropriate amount of 0.1 mol dm^{-3} NaOH or HNO_3 to obtain the desired pH. Adsorption studies were carried out by agitating 25 cm^3 of a known concentration of RhB solution with 50 mg of adsorbent at a fixed temperature (20 °C) for 24 h in stoppered glass bottles. The mixtures were filtered by gravity, and the final concentration of RhB in the filtrate was determined at 554 nm (λ_{max} of RhB) by means of ultraviolet-visible (UV-vis) spectrophotometry. The effect of pH, adsorbent dose, temperature and initial RhB concentration were studied for each adsorbent to determine the optimum conditions necessary for adsorption. The adsorption efficiency (% adsorbed) and adsorption capacity (q_e) were calculated by using equations 1 and 2 respectively.

$$\% \, adsorbed = \left(\frac{C_i - C_{eq}}{C_i} \right) \times 100 \qquad (1)$$

$$q_e = \left(\frac{C_i - C_{eq}}{m} \right) \times V \qquad (2)$$

where C_i is the initial RhB concentration (mg dm^{-3}), C_{eq} is the equilibrium concentration of RhB (mg dm^{-3}), q_e is the adsorption capacity (mg g^{-1}), m is the mass (mg) of the adsorbent and V is the volume (dm^3) of the adsorbate solution used.

2.7.1. Kinetics studies

Kinetics studies were investigated by contacting 25 cm^3 of 100 mg dm^{-3} RhB solution with 50 mg of adsorbent at pH 7 in stoppered glass bottles. The solutions were agitated in a thermostated shaking water bath at 20 °C for different time intervals in the range of 5-1440 min. After the pre-determined time intervals, the samples were filtered and the final concentrations of RhB determined spectrophotometrically. The experimental adsorption data were applied to the pseudo-first order, pseudo-second order, intraparticle diffusion and Elovich kinetics models given in Table 2.

[Insert Table 2]

2.7.2. Adsorption isotherms

Solutions of RhB with initial concentrations ranging from 10-100 mg dm^{-3} were prepared at a constant pH of 7. Aliquots of 25 cm^3 were mixed with 50 mg of the adsorbent and agitated in a thermostated shaking water bath at 20-45 °C for 24 h in stoppered glass bottles. The solutions were filtered and the concentrations of RhB in the filtrates determined spectrophotometrically. The experimental adsorption equilibrium data were analysed by the adsorption models given in Table 3.

[Insert Table 3]

2.7.3. Desorption experiments

Desorption studies were investigated by first contacting aliquots of 25 cm^3 of 100 mg dm^{-3} RhB solution with 50 mg of adsorbent. The solutions were agitated on a thermostated shaking water bath at 20 °C for 24 h. After agitation, the solutions were filtered and the equilibrium concentration of RhB in the filtrates was determined. The RhB-loaded adsorbent was dried in a vacuum oven at 80 °C. The 50 mg of the RhB-loaded adsorbent was weighed

and subsequently agitated with either a 10 cm^3 aliquot of acetone or ethanol for 30 min. The final concentration of RhB desorbed was then obtained from the filtrates collected.

2.8. Data Analysis

Experimental data were fitted to the kinetics and isotherm models by means of the nls nonlinear regression routine in the R statistical computing environment.[47] In the case of all models chosen, an examination of the residuals was performed in order to assess the adequacy of the model.

3. Results and discussion

The adsorbents synthesized were characterized by a number of different techniques to confirm that the materials obtained would be effective for adsorption. A comparison of the efficiency of these adsorbents for RhB removal was investigated at varying conditions by means of batch adsorption experiments.

3.1. Characterization of adsorbents

The FTIR study of acid-functionalized CNTs (MWCNT-COOH) confirmed the presence of C=C, C=O, CH_2, C-O and O-H functional groups, demonstrating the successful introduction of O-containing groups on the tubes (Fig. 1). As reported by Buang *et al.*,[48] O-H and C=O functional groups are usually produced after oxidation of pristine MWCNTs. The peaks at 3200 cm^{-1} (O-H stretching mode), 1635-1700 cm^{-1} (C=O stretching mode), 1452-1600 cm^{-1} (C=C stretching mode), and 2200-2500 cm^{-1} (oxygen containing groups such as lactonic and anhydride groups), are evidence of functionalization of MWCNTs.[36] These peaks remained

present in the spectra of the nanocomposites containing MWCNT-COOH. Fig. 1 further shows the FTIR spectra of the $CoFe_2O_4$ nanoparticles and CNT-$CoFe_2O_4$ nanocomposites. The spectra of the $CoFe_2O_4$ nanoparticles were observed to show sharp intense peaks at 560 cm^{-1} which are usually associated with metal-oxygen (Fe(Co)-O) stretching vibrations in the ferrite lattice which is in agreement with previously published data.[36,49,50] These peaks, at about 560 cm^{-1}, remained present in composites, although a shift in the Fe(Co)-O peaks to higher wavenumber was noticed. The shift could be attributed to interactions between the ferrites and MWCNT-COOH through O-containing functional groups.[36] The presence of these peaks demonstrates that nanocomposites containing MWCNT-COOH and ferrites were successfully synthesized. The intensity of the Fe(Co)-O stretching vibrations was noticed to decrease as the percentage of MWCNT-COOH increased in composites. This indicates that the percentage of the more abundant material determines the intensity of the peaks obtained in the FTIR spectra.

[Insert Fig 1]

To observe the structure and size distribution of the nanomaterials produced, images were collected from TEM and HRTEM. Fig. 2 shows HRTEM images of (a) MWCNT-COOH, (b) $CoFe_2O_4$ nanoparticles and (c) 29 % composite, while Fig. 3 shows TEM images of (a) 29 % and (b) 75 % nanocomposites at the same magnification. It was observed that the tubular-shaped structure characteristic of MWCNTs was preserved after functionalization was carried out (Fig 2a), however, functional groups such as –COOH are not usually visible on HRTEM micrographs. Uniform cubic-shaped materials were obtained for the $CoFe_2O_4$ nanoparticles with a high degree of agglomeration as demonstrated with arrows in Fig. 2b. Similarly, a high degree of agglomeration of $CoFe_2O_4$ nanoparticles was noticed on the sides of tubes.

The tubular structure of CNTs was also preserved for all synthesised nanocomposites (see Fig. 3). It was also noticed that the amount of agglomerated $CoFe_2O_4$ nanoparticles reduces as the percentage of MWCNT-COOH increases in the composites (Fig 3a vs 3b). Similar trends have been reported for ferrites[51] and magnetic carbon nanotubes[49,52] in previous studies. This therefore demonstrates that nanocomposites containing MWCNTs and $CoFe_2O_4$ nanoparticles were successfully synthesized, since the cubic shape of ferrites and the tubular structures of MWCNTs were preserved in the nanocomposites.

[Insert Figs 2 and 3]

The surface area and porosity of nanomaterials is usually obtained by applying the Brunauer, Emmett and Teller (BET) and the Barrett-Joyner-Halenda (BJH) theories respectively. $CoFe_2O_4$ nanoparticles and CNTs have been reported to have moderately large surface areas.[34,46,53] and is confirmed in this work as demonstrated in entries 1 and 2 of Table 4. Oxidation of purified MWCNTs with acids introduces defects and shortening of tubes, thereby increasing the surface area of MWCNT-COOH.[41,54] The extent of disorder/defects and crystallinity of MWCNTs was evaluated with the use of Raman spectroscopy. The most characteristic peaks usually observed are the D band (1350 cm^{-1}) and G band (1580 cm^{-1}). The D band (I_D) gives information on the disorder-induced modes and defects in the graphene sheets at the walls of the tubes, while the G band (I_G) gives information on the crystalline graphitic arrangement on the MWCNTs.[55] The relative intensity ratio of the bands (I_D/I_G) was calculated. A larger ratio indicates a greater disruption of the sp^2 hybridized atoms to the sp^3 hybridized atoms, hence, interpreted as a high defect/deformation occurring on the walls/sides of the tubes.[54] Raman spectroscopic measurements performed on the MWCNTs indicate that the I_D/I_G ratio increased after functionalization with acids (entry 3 vs 2, Table 4).

This could be due to the fact that oxidation of MWCNTs increases the defects and decreases the graphitic structure of the tubes resulting in a larger I_D/I_G ratio being obtained.[41,46,54] An increase in the surface area of MWCNT-COOH to 126.8 m^2 g^{-1} was measured after functionalization (entry 3 vs 2 of Table 4). A further increase in the surface area of the adsorbents was achieved by preparing composites containing varying percentages of $CoFe_2O_4$ and MWCNT-COOH. An increase in the surface area of nanocomposites synthesized from MWCNTs and iron nanoparticles was similarly reported by Gong *et al.*[56] It was further observed that the BET surface area, pore volume and pore diameter of the composites increased with an increase in the MWCNT-COOH content (entries 4-6, Table 4). The pore volume of these materials was noticeably increased from 0.40 to 1.16 cm^3 g^{-1} which could further aid in the availability of more active sites. Hence, the materials produced in this study possess moderately large surface areas with reasonable pore volumes and should exhibit good adsorption properties.

[Insert Table 4]

3.2. Batch adsorption experiments

The adsorption of RhB by $CoFe_2O_4$, MWCNT-COOH and CNT-$CoFe_2O_4$ nanocomposites was investigated for the efficient remediation of polluted wastewater. The adsorption capacity of the adsorbents was compared to determine the adsorbent with the best efficiency for RhB removal. Factors such as pH, contact time, initial RhB concentration, adsorbent dose and temperature were varied in order to attain the optimum conditions for RhB adsorption. Desorption studies for all the adsorbents were also carried out to examine the feasibility of regenerating the used adsorbents for further use.

3.2.1. Effect of pH

The pH of a solution can affect the surface charge on a particular adsorbent and the charge of the adsorbate.[27] The influence of pH on adsorbents was investigated by agitating a known concentration of RhB solution for 24 h with an adsorbent dose of 50 mg. The solutions were adjusted to obtain an initial pH value in the range of 1-10. Fig. 4 shows that the adsorption of RhB onto all adsorbents was greatly influenced by the pH of the solution. At low pH values, RhB is cationic and therefore adsorption onto the protonated adsorbents was minimal; however, an increase in efficiency was noticed as the solution was changed to basic. With increasing pH from 1.0 to 10.0, interactions between RhB and the negatively charged surface groups on the adsorbents increased, with optimum conditions obtained at pH 6-8 for all adsorbents (Fig 4). At this pH, RhB assumes the quinonoid structure (i.e. it exists in the zwitterion form).[57] As stated by Salleha et al.,[1] cationic adsorption is favoured when the pH of the solution is greater than the point of zero charge (pH_{PZC}). This statement concurs with these results since as illustrated in Table 4; the pH_{PZC} values measured are lower than the optimum pH condition obtained for each adsorbent. This fact supports that electrostatic interaction between the RhB zwitterion and the negatively charged surface of the adsorbents is responsible for adsorption. However, it is also worthy of note that with increasing pH the dissociation of the aromatic carboxylic acid group in RhB will increase as will deprotonation of the nitrogen groups, thereby increasing electrostatic repulsion between RhB and the negatively charged adsorbents. Fig 4 demonstrates this effect that an increase in the basicity of the solution (i.e. pH > 8) results in a decrease in adsorption capacity (q_e) of the adsorbents. Similar observations were reported by Annadurai *et al*.[58] and Zhang *et al.*[20] for RhB removal. This therefore suggests that adsorption is primarily influenced by electrostatic interaction

between the RhB zwitterion and the adsorbents; however, other factors such as the molecular structure of the adsorbate might also influence adsorption.

Although, the adsorption capacity was best for the MWCNT-COOH, in the case of the nanocomposites it was noticeably increased as the percentage of MWCNT-COOH increased. This could be as a result of the increase in the number of defects (as observed in the increasing I_D/I_G ratio shown in Table 4) and the presence of a greater number of oxygen-containing functional groups introduced by chemical oxidation of the MWCNTs. Both of these create more active sites for electrostatic interaction and hence enhance adsorption (Fig. 4). All further adsorption experiments were carried out at a pH value of 7, since this value falls within the optimum range for all the adsorbents considered in this work.

[Insert Fig 4]

3.2.2. Effect of contact time

In order to obtain the contact time required to achieve equilibrium, the experimental investigation of the adsorption of RhB from aqueous solutions onto $CoFe_2O_4$, MWCNT-COOH and CNT-$CoFe_2O_4$ nanocomposites was performed for different time intervals. Fig. 5 shows that the adsorption capacity (q_e) of RhB onto all adsorbents increases as the contact time increases. For all adsorbents, sorption was rapid in the first 360 min owing to the fact that more sites were available for adsorption on the adsorbents, creating room for fast interaction between the adsorbent and adsorbate. As the process continues, adsorption sites become limited and the rate of adsorption is influenced by the speed at which the adsorbates move from the external to the internal sites of the adsorbent particles. The faster it takes to reach equilibrium, the better an adsorbent is. It is noticed that as the time increases (beyond

360 min), adsorption reaches a state of equilibrium, hence, adsorption was seen to slow down at this time due to saturation of active sites on the adsorbents. It could therefore be said that the equilibrium time for all adsorbents in this study was achieved at 6 h. However, in this study, an equilibration time of 24 h was used to ascertain the complete removal of RhB under all conditions.[18]

Fig. 5 further demonstrates that for the nanocomposites, the adsorption capacity was enhanced as the amount of MWCNT-COOH was increased. This is clearly explained by the fact that as the content of MWCNT-COOH in the composites increases; more negative sites are introduced, therefore favouring adsorption.

[Insert Fig 5]

3.2.3. Adsorption kinetics

The mechanism and rate-determining step of adsorption of RhB onto $CoFe_2O_4$, CNT-$CoFe_2O_4$ nanocomposites and MWCNT-COOH was investigated by fitting the Lagergren pseudo-first order,[59] pseudo-second order,[60] intraparticle diffusion[61] and Elovich models[62] to the kinetics data. The equations for these models are given in Table 2. Adsorption usually occurs through four processes: diffusion of the adsorbate from the bulk solution onto the surface of the adsorbent, the passage of adsorbate through the liquid film attached to the surface of the adsorbent (film diffusion), diffusion of adsorbate through the pores of the adsorbent (intraparticle diffusion) and interaction of the adsorbate with the active sites on the adsorbate.[18] The dependence of the model which best fits the experimental data was determined based on the model with lowest value for the sum of squared residuals (SSR) and the residual standard error (RSE). Based on these estimates, the kinetics data obtained were

best described by the pseudo-second order model (Table 5). The model is based on the assumption that adsorption occurs through bimolecular interactions involving sharing or exchange of electrons between RhB and the adsorbent.

Considering that various mechanisms usually control adsorption kinetics, the intraparticle diffusion model was also utilized to explain the rate-limiting step of the process. A plot of q_e versus $t^{1/2}$ is usually indicative of the multistep-controlling processes of adsorption.[32] Adsorption is assumed to proceed only through intraparticle diffusion if a linear plot which also passes through the origin is obtained. It is, however, assumed that the process is controlled by two or more steps if a linear plot which does not pass through the origin is obtained.[63-65] Plots obtained from this study produced linear plots, which do not pass through the origin. Therefore, these results suggest that though adsorption proceeded *via* intraparticle diffusion, it was not the only rate-controlling step for the process. The plots further illustrate that the adsorption of RhB proceeded through transportation of RhB to the external surface of the adsorbent by film diffusion, followed by intraparticle diffusion of RhB to the pores of the adsorbent, and subsequently intraparticle diffusion slows down due to the low RhB concentration.[63-65] Thus a multi-step process is involved. The intraparticle diffusion constant (k_{id}) and boundary layer (l) were obtained from the slope and intercept of the plots respectively. Data obtained for k_{id} and l show an increase with the addition of MWCNT-COOH to the composites (Table 5). These results demonstrate that adsorption was boundary-layer controlled for all adsorption processes. Increasing amounts of MWCNT-COOH in the adsorbents resulted in an increase in the boundary thickness (l); hence resulting in higher adsorption capacities (q_e) obtained (Table 5).

[Insert Table 5]

3.2.4. Effect of adsorbent dose

To evaluate the adsorption capacity for RhB, the mass of each adsorbent was varied from 30 to 400 mg. An increase in the adsorption capacity (q_e) was observed as the mass of adsorbent is increased (Fig. 6). In fact, it was observed that 100 % removal efficiency was achieved for some adsorbents when the dose was increased to 400 mg. This is due to the fact that as the mass of adsorbent is increased, the surface area available for adsorption increases, thereby creating more active sites for adsorption. Table 4 demonstrates that the pore volume is lowest in $CoFe_2O_4$ and increases as more MWCNT-COOH content was added to the composites. The increase in the adsorption capacity (q_e) for the same mass of adsorbent (Fig. 6) could be as a result of the increase in pore volume which enabled greater removal of RhB as the MWCNT-COOH content is increased. Hence, surface area and pore volume of adsorbents plays a major role in enhancing the capacity of adsorbents in adsorption. However, adsorption was noticed to reach a constant value where further adsorption becomes negligible with increase in adsorbent mass due to the limited amount of RhB available. Again, the amount of RhB adsorbed was in the same order as the percentage content of MWCNT-COOH.

[Insert Fig 6]

3.2.5. Effect of initial RhB concentration

To effectively explain the increase in the activities (q_e) of each adsorbent, different concentration ranges with the same amount of adsorbent were used. Generally, it was observed that as the concentration of adsorbate increases, the adsorption capacity (q_e) increased for a fixed quantity of adsorbent while the percentage adsorption decreased. At

low adsorbate concentrations, more active sites are available on the adsorbent; hence the removal efficiency is high. The increase in adsorption capacity with an increase in the initial concentration of adsorbate is as a result of an increase in the driving force due to the concentration gradient developed between the bulk solution and the surface of the adsorbent. However, at higher concentrations, the active sites of adsorbents become saturated with RhB molecules as the process continues. Hence, this process led to a decrease in the percentage adsorption and an increase in the uptake of the adsorbate (q_e) by the adsorbents as the concentration is increased.

3.2.6. Effect of temperature

The adsorption of RhB onto each adsorbent was investigated at 293, 303, 313 and 318 K. An increase in the adsorption capacity of RhB was observed with increase in temperature from 293 to 318 K for $CoFe_2O_4$, and the 29 % and 75 % composites, and MWCNT-COOH (Fig 7 a-b, d-e). This indicates the endothermic nature of the adsorption process. As the temperature increases, the kinetic energy of the RhB molecules increases, resulting in enhancement of the rate of adsorption. Also, an increase in temperature could result in an increase in the pore volumes of the adsorbents, enabling an increase in the active sites available for adsorption.[27,31] However, a marked difference was observed for the composite produced with a 50 % dosage of MWCNT-COOH in $CoFe_2O_4$. An exothermic adsorption process was observed for this adsorbent (see Fig. 7c), i.e. the extent of adsorption decreased with an increase in temperature.

[Insert Fig 7]

3.2.7. Adsorption isotherms

Isotherm models provide information on the capacity of adsorbents or the amount needed to remove a unit mass of pollutant under the same conditions. Eight models, including various two-parameter (Freundlich,[66] Langmuir,[67] Temkin,[68] Dubinin-Radushkevick[69]) and three-parameter (Sips,[70] Khan,[71] Redlich-Peterson,[72] Toth[73]) isotherms, were applied to the equilibrium data obtained. The equations of the tested models are given in Table 3. Tables 6-8 give the calculated isotherm parameters for all the models tested. The model which best describes the equilibrium data was chosen based on the lowest SSR value.

Table 9 summarizes the parameters of the models which best fit the equilibrium data obtained for each adsorbent. Results obtained indicated that the Langmuir isotherm, which assumes monolayer adsorption onto homogeneous surfaces with a finite number of identical adsorption sites,[67] is the best of the models considered for $CoFe_2O_4$, MWCNT-COOH and the 50 % nanocomposite. Results further demonstrated that the Langmuir isotherm is the best of the two-parameter models considered and the Sips model, which is a combination of the Langmuir and Freundlich isotherms,[70] is the best of the three-parameter models for 29 % and 75 % MWCNT-$CoFe_2O_4$ nanocomposites. This implies that the uptake of RhB onto the active sites of the adsorbents occurs on uniform and equivalent sites, wherein there exists no interaction between adjacent adsorbate ions. The value of *b* (Table 9) gives an indication of the binding power (i.e. adsorptive strength) between adsorbent and adsorbates. An increase in adsorptive strength (*b*) was obtained with increasing amounts of MWCNT-COOH in the composites (Table 9). This further elucidates that strong interactions were formed between RhB and the adsorbents as the content of MWCNT-COOH increases.

[Insert Tables 6-9]

3.2.8. Thermodynamic parameters of adsorption

The quantity adsorbed at each temperature was examined to obtain the thermodynamic parameters of adsorption. The change in Gibbs energy, $\Delta G°$, was calculated from equation (3):[74]

$$\Delta G° = -RT ln\, K \quad (3)$$

where $\Delta G°$ is the standard Gibbs energy change in J mol^{-1}, R is the gas constant (8.314 J K^{-1} mol^{-1}), T is the temperature in Kelvin and K was obtained from the product of q_m and b obtained from the Langmuir plot (Table 9).[18,75] The value of K was corrected to be dimensionless by multiplying by a factor of 1000.[76]

A linear plot of ln K against $1/T$ was obtained from which the slope and intercept correspond to the value of the change in enthalpy, $\Delta H°$, and change in entropy, $\Delta S°$, respectively, according to the Van't Hoff equation (eqn 4):[74]

$$\ln K = -\frac{\Delta H°}{RT} + \frac{\Delta S°}{R} \quad (4)$$

Negative values were obtained for $\Delta G°$ indicating the spontaneous and feasible nature of the adsorption of RhB onto the adsorbents investigated (Table 10). It was also noticed that the negative values increase with an increase in temperature indicating better adsorption as the temperature is increased. The $\Delta S°$ values for all adsorbents were observed to be positive indicating an increase in the degree of disorderliness of the system as temperature is increased. This result demonstrates that adsorption was entropy-driven for all adsorbents in this study since an endothermic enthalpy of adsorption was observed for most of the adsorbents. Adsorbates can interact with the surface of an adsorbent through physical interaction (physisorption) or chemical sorption (chemisorption). When the heat of

adsorption is between 2.1 to 20.9 kJ mol^{-1}, a physisorption process is assumed to occur while chemisorption could be said to occur when the heat of adsorption is between 80 to 200 kJ mol^{-1}.[18,77] However, as noticed from Table 10, the values of $\Delta H°$ show that for $CoFe_2O_4$ and the 50 % nanocomposite, RhB was physisorbed to the surface of the adsorbents while for the MWCNT-COOH, 29 % and 75 % nanocomposites the interaction could be a physio-chemical process, since the $\Delta H°$ values were higher than for a physisorption process, but lower than for chemisorption.[18,77] This demonstrates that adsorption of RhB onto the adsorbents studied could be as a result of interaction of the adsorbent and adsorbate *via* the formation of a strong ionic bond (chemisorption) and interaction through weaker van der Waals forces between the adsorbate and adsorbents (physisorption). It is worthy of note that the 50 % dosage nanocomposite displayed an exothermic $\Delta H°$. This shows that though adsorption was spontaneous, the reaction was exothermic in nature and hence for this adsorbent, enthalpy was the driving factor.

[Insert Table 10]

The Langmuir adsorption capacities (q_m) of adsorbents were compared with those obtained from previously published data (Table 11) for the removal of RhB from simulated wastewater. The table illustrates that the uptake (q_e) of adsorbents used in this study compares favourably with previously obtained data. An increase in the efficiency of adsorbents was achieved with an increase in carbon-based materials which resulted in the increase in the adsorption capacities (q_m).

[Insert Table 11]

3.3. Desorption Studies

Desorption studies were carried out to determine the reusability of the adsorbents tested, by agitating 50 mg of the RhB-loaded sample with either 10 cm^3 of ethanol or acetone. It is important to ascertain whether used adsorbents can be regenerated and made effective for reuse. In this way the discharge of secondary pollutants into the environment is hindered in that the spent adsorbents are recycled for reuse and not disposed directly after usage. The adsorbate (in this case the RhB dye) can also be recovered for reuse. The experimental results (Table 12) show a good desorption efficiency of RhB by using either ethanol or acetone. Acetone was found to better desorb the dye with efficiencies between 80 and 95 %. Characterization of the regenerated adsorbents was carried out and the results were found to be similar to those obtained with freshly prepared unused adsorbents, therefore confirming the reusability. Hence, all adsorbents used in this study can be regenerated for reuse.

[Insert Table 12]

4. Conclusions

Adsorption of RhB from aqueous solution was successfully carried out by using $CoFe_2O_4$ nanoparticles, MWCNT-COOH, and CNT-$CoFe_2O_4$ nanocomposites. Characterization of the adsorbents confirmed the presence of functional groups available for interaction with RhB. Based on the experimental results obtained, it was observed that the adsorption capacity of adsorbents to remove RhB significantly increased from 5.165 to 42.68 mg g^{-1} with increasing MWCNT-COOH content. The highest adsorption capacity was obtained with MWCNT-COOH as adsorbent, however, CNT-based nanocomposites showed better capacities than $CoFe_2O_4$ nanoparticles. This study therefore demonstrates that the incorporation of carbon-based nanomaterials, such as MWCNTs, can improve the textural characteristics and

adsorption capacity of $CoFe_2O_4$, thereby, making them suitable adsorbents for wastewater remediation.

The maximum removal of RhB from a simulated wastewater was achieved at an optimum pH of 7, and equilibrium was reached after 360 min. The kinetics of adsorption followed the pseudo-second order model indicating a bimolecular rate-determining step. The equilibrium data was better described by the Langmuir isotherm model indicating monolayer coverage of RhB onto the homogeneous sites of the adsorbents. An increase in the adsorption capacity was achieved as the temperature of the solution was increased except for the 50 % nanocomposite. This factor makes these adsorbents useful in the treatment of effluents discharged directly from industries since these are typically above ambient temperatures. The adsorption process was thermodynamically spontaneous and entropy-driven for the adsorbents except for the 50 % nanocomposite. The adsorbed RhB was efficiently desorbed with either ethanol or acetone, but the latter showed the highest desorption capacity. Thus, these adsorbents show potential for reuse and do not create a secondary pollutant problem.

We therefore infer that electrostatic interaction between RhB and the adsorbents was primarily responsible for adsorption in this study. The interactions between the adsorbate and adsorbents were strong, indicating both physisorption and chemisorption processes. It is worthy of note that though MWCNT-COOH showed the best adsorption capacity, the nanocomposites provide an advantage of magnetic separation, which limits problems associated with removal of adsorbents from aqueous media. This study, therefore, demonstrates that cobalt ferrite nanoparticles, multiwalled carbon nanotubes, and CNT-based nanocomposites provide potential applications for the removal of pollutants from the

environment through adsorption. Furthermore, the synthesized nanocomposites were found to be stable, durable and hence reusable for RhB adsorption.

Acknowledgements

The authors wish to thank the University of KwaZulu-Natal, Durban for research facilities and the National Research Foundation (NRF) for provision of funds for the completion of this work.

References

1. M. A. M. Salleha, D. K. Mahmoud, W. A. A. Karim and A. Idris, *Desalination*, 2011, **280**, 1-13.
2. T. Robinson, G. McMullan, R. Marchant and P. Nigam, *Bioresour. Technol.*, 2001, **77**, 247-255.
3. Sumanjit, S. T. P. Walia and I. Kansal, *J.Surf. Sci. Technol.*, 2008, **24**, 179-193.
4. A. Y. Zahrim and N. Hilal, *Water Res. Ind.*, 2013, **3**, 23-34.
5. V. P. Kasperchik, A. L. Yaskevich and A. V. Bildyukevich, *Petrol. Chem.*, 2012, **52**, 545-556.
6. S. Nadupalli, N. Koorbanally and S. B. Jonnalagadda, *J. Phys. Chem. A*, 2011, **115**, 11682-11688.
7. O. Türgay, G. Ersöz, S. Atalay, J. Forss and U. Welander, *Sep. Purif. Technol*, 2011, **79**, 26-33.
8. S. Nadupalli, N. Koorbanally and S. B. Jonnalagadda, *J. Phys. Chem A*, 2011, **115**, 7948-7954.
9. A. Rezaee, M. T. Ghaneian, A. Khavanin, S. J. Hashemian, G. Moussan, G. Ghanizadeh and E. Hajizadeh, *Iranian J. Environ.Health Sci. Eng.*, 2008, **5**, 95-100.
10. B. Pare, B. Bhawna Sarwan and S. Jonnalagadda, *Appl. Surf. Sci.*, 2011, **258**, 247 - 253.
11. A. Ahmad, W. Harris, Syafiie and O. Seng, *Jurnal Teknologi*, 2002, **36**, 31-44.
12. L. Wojnarovits and E. Takacs, *Radiat. Phys. Chem.*, 2008, **77**, 225-244.
13. K. Murugesan and P. T. Kalaichelvan, *Indian J. Exp Biol*, 2003, **41**, 1076-1087.
14. M. A. García-Morales, G. Roa-Morales, C. Barrera-Díaz, V. Martínez Miranda, P. Balderas Hernández and T. B. Pavón Silva, *Int. J. Electrochem Sci.*, 2013, **8**, 8752-8763.
15. P. Dachipally and S. B. Jonnalagadda, *J. Environ. Sci. Health., Part A*, 2011, **46**, 887-897.
16. Y. Yan, M. Zhang, K. Gong, L. Su, Z. Guo and L. Mao, *Chem. Mater.*, 2005, **17**, 3457-3462.
17. S. B. Jonnalagadda and S. Nadupalli, *Talanta*, 2004, **64**, 18 - 22.
18. I. A. A. Hamza, B. S. Martincigh, J. C. Ngila and V. O. Nyamori, *Phys. Chem. Earth*, 2013, **66**, 157-166.
19. Y. Li, Q. Du, T. Liu, X. Peng, J. Wang, J. Sun, Y. Wang, S. Wu, W. Z, Y. Xia and L. Xia, *Chem. Eng. Res. Des.*, 2013, **91**, 361-368.
20. Z. Zhang, I. M. O'Hara, G. A. Kent and W. O. S. Doherty, *Ind. Crop Prod.*, 2013, **42**, 41-49.
21. R. Gong, Y. Sun, J. Chen, H. Liu and C. Yang, *Dyes Pigments*, 2005, **67**, 175-181.

22. M. C. Akkaya, S. Emik, G. Guclu, B. T. Iyim and S. Ozgumus, *J. Appl. Polym. Sci.*, 2009, **114**, 1150-1159.
23. S. H. Kareem and Al-Hussien, *J. Baghdad Sci.*, 2012, **9**, 680-688.
24. C. C. Wang, L. C. Juang, T. C. Hsu, C. K. Lee, J. F. Lee and F. C. Huang, *J. Colloid Interface Sci.*, 2004, **273**, 80-86.
25. O. S. Bello, O. A. Olusegun and V. O. Njoku, *B. Chem Soc. Ethiopia*, 2013, **27**, 191-204.
26. S. Wang, Y. Boyjoo, A. Choueib and Z. H. Zhu, *Water Res.*, 2005, **39**, 129-138.
27. T. A. Khan, S. Dahiya and I. Ali, *Appl. Clay Sci.*, 2012, **69**, 58-66.
28. Mundhe K. S., Gaikwad A. B., Torane R. C., Deshpande N. R. and K. R. V., *J. Chem. Pharm. Res.*, 2012, **4**, 423-463.
29. G. Guclu, *Desalination*, 2010, **259**, 53-58.
30. T. B. Iyim, I. Acar and S. Ozgumus, *J. Appl. Polym. Sci.*, 2008, **109**, 2774-2780.
31. T. A. Khan, M. Nazir and E. A. Khan, *Toxicol. Environ. Chem.*, 2013, **95**, 919-931.
32. P. Parimaladevi and V. Venkateswaran, *J. Appl. Technol. Environ. Sanit.*, 2011, **1**, 285-293.
33. C. Namasivayam, N. Muniasamy, K. Gayatri, M. Rani and K. Ranganathan, *Bioresour. Technol.*, 1996, **57**, 37-43.
34. L. Wang, J. Li, Y. Wang, L. Zhao and Q. Jiang, *Chem. Eng. J.*, 2010, **181-182**, 72-79.
35. R. Jiang, Y. Q. Fu, H. Y. Zhu, J. Yao and L. Xiao, *J. Appl. Polym. Sci.*, 2012, **125**, E540-E549.
36. L. Ai, C. Zhang, F. Liao, Y. Wanga, M. Li, L. Meng and J. Jiang, *J. Hazard. Mater.*, 2011, **198**, 282-290.
37. S. Iijima, *Nature*, 1991, **354**, 56-58.
38. B. Pan and B. Xing, *Environ. Sci. Technol.*, 2008, **42**, 9005-9013.
39. C. Lu, Y.-L. Chung and K.-F. Chang, *Water Res.*, 2005, **39**, 1183-1189.
40. K. Balasubramanian and M. Burghard, *Small*, 2005, **1**, 180-192.
41. V. Datsyuk, M. Kalyva, K. Papagelis, J. Parthenios, D. Tasis, A. Siokou, I. Kallitsis and C. Galiotis, *Carbon*, 2008, **46**, 833-840.
42. J. Shen, W. Huang, L. Wu, Y. Hu and M. Ye, *Mater. Sci. Eng., A* 2007, **464**, 151-156.
43. C. Lu and H. Chiu, *Chem. Eng. Sci.*, 2006, **61**, 1138-1145.
44. K. McDonough, J. L. Fairey and G. V. Lowry, *Water Res.*, 2008, **42**, 575-584.
45. K. Maaz, A. Mumtaz, S. K. Hasanain and A. Ceylan, *J. Magn. Magn Mater.* , 2007, **308**, 289-295.
46. S. Santangelo, G. Messina, G. Faggio, S. H. Abdul Rahim and C. Milone, *J. Raman Spectrosc.*, 2012, **43**, 1432-1442.
47. The R development core team, *R version 3.0.2* 2013.

48. N. A. Buang, F. Fadil, A. Abdul Majid and S. Shahir, *Dig. J. Nanomater. Bios.* , 2012, **7**, 33-39.
49. A. K. Mishra and S. Ramaprabhu, *J. Phys. Chem.C*, 2010, **114**, 2583-2590.
50. L. Kong, X. Lu and W. Wanjin Zhang, *J. Solid State Chem.*, 2008, **181**, 628-636.
51. Y.-Y. Xu, M. Zhou, H.-J. Genga, J.-J. Haoa, Q.-Q. Oua, S.-D. Qia, H.-L. Chen and X.-G. Chen, *Appl. Surf. Sci.*, 2012, **258**, 3897-3902.
52. B. Jia and L. Gao, *J. Phys. Chem. B*, 2007, **111**, 5337-5343.
53. A. Afkhami and R. Moosavi, *J. Hazard. Mater.*, 2010, **174**, 398 - 403.
54. Z. Zhao, Z. Yang, H. Y., J. Li and X. Fan, *Appl. Surf. Sci.*, 2013, **276**, 476-481.
55. Y. Zhang, H. He, C. Gao and J. Wu, *Langmuir* 2009, **25**, 5814-5824.
56. J.-L. Gong, B. Wang, G.-M. Zeng, C.-P. Yang, C.-G. Niu, Q.-Y. Niu, W.-J. Zhoua and Y. Liang, *J. Hazard. Mater.*, 2009, **164**, 1517-1522.
57. Canadian Environmental Protection Agency, *Chemical Abstracts Service Registry Number*, 2010, **509-34-2**.
58. G. Annadurai, R.-S. Juang and D.-J. Lee, *J.Hazard. Mater.*, 2002, **B92**, 263-274.
59. Y. S. Ho, *Water Res.*, 2004, **38**, 2962-2964
60. Y. S. Ho and G. McKay, *Process Saf. Environ.Prot*, 1998, **76**, 183-191.
61. E. Demirbas, M. Kobya, E. Senturk and T. Ozkan, *Water S.A.*, 2004, **30**, 533-539.
62. S. H. Chien and W. R. Clayton, *Soil Sci. Soc. of Am. J.*, 1980, **44**, 265-268.
63. Y. Yao, F. Xu, M. Chen, Z. Xu and Z. Zhu, *Bioresour. Technol.*, 2010, **101**, 3040-3046.
64. C. H. Wu, *J. Hazard. Mater.*, 2007, **144**, 93-100.
65. S. G. Muntean, M. E. Radulescu-Grad and P. Sfarloaga, *RSC Adv.*, 2014, **4**, 27354-27362.
66. H. Freundlich, *Z Phys. Chem.*, 1906, **57**, 385-470.
67. I. Langmuir, *J. Am. Chem. Soc.*, 1918, **40**, 1361-1402.
68. M. I. Temkin and V. Pyzhev, *Acta Phys. Chim*, 1940, **12**, 327-356.
69. M. M. Dubinin and L. V. Radushkevich, *Proc. Natl. Acad. Sci.*, 1947, **55**, 327-329.
70. R. Sips, *J. Chem. Phys*, 1948, **16**, 490-495.
71. A. R. Khan, I. R. Al-Waheab and A. Al-Haddad, *Environ. Technol.*, 1996, **17**, 13-23.
72. O. Redlich and D. L. Peterson, *J. Phys. Chem*, 1959, **63**, 1024.
73. J. Toth, *Acta Chim. Acad. Sci. Hung.*, 1971, **69**, 311-328.
74. K. M. Doke and E. M. Khan, *Rev.Environ. Sci. Bio.*, 2013, **12**, 25-44.
75. R. Djeribi and Q. Hamdaoui, *Desalination*, 2008, **225**, 95-112.
76. S. K. Milonjić, *J. Serb. Chem. Soc.*, 2007, **72**, 1363-1367.
77. Y. Liu and Y.-J. Liu, *Sep. Purif. Technol.*, 2008, **61**, 229-242.

78. Y.-S. Ho, *Water Res.*, 2003, **37**, 2323-2330.

79. J. Lin and L. Wang, *Front. Environ. Sci. En.*, 2009, **3**, 320-324.

80. S. Kumar, G. Bhanjana, K. Jangra, N. Dilbaghi and A. Umar, *J. Nanosci. Nanotechno.*, 2014, **14**, 4331-4336.

81. K. Kerkez and S. S. Bayazit, *J. Nanopart. Res.*, 2014, **16**, 2431-2441.

82. V. K. Gupta, R. Jain, M. N. Siddiqui, T. A. Saleh, S. Agarwal, S. Malati and D. Pathak, *J. Chem. Eng. Data*, 2010, **55**, 5225-5229.

83. T. Madrakian, A. Afkhami, H. Mahmood-Kashani and M. Ahmad, *Iran Chem. Soc.*, 2013, **10**, 481-189.

84. L. Peng, P. Qina, M. Lei, Q. Zeng, H. Song, J. Yang, J. Shao, B. Liao and J. Gua, *J. Hazard. Mater.*, 2012, **209-210**, 193-198.

Table 1: Adsorbent composition/identification

	% Composition by mass	
Sample Identifier	**$CoFe_2O_4$**	**MWCNT-COOH**
$CoFe_2O_4$	100	0
29 %	71	29
50 %	50	50
75 %	25	75
MWCNT-COOH	0	100

Table 2: Kinetics models investigated for the adsorption of RhB onto $CoFe_2O_4$, MWCNT-COOH, and CNT-$CoFe_2O_4$ composites

Model	Equation	Parameters†	References
Pseudo-first order	$q_t = q_{eq}(1 - e^{-k_1 t})$	q_{eq}, k_1	59, 78, 79
Pseudo-second order	$q_t = \frac{k_2 q_{eq}^2 t}{1 + k_2 q_{eq} t}$	k_2, q_{eq}	60, 78, 79
Elovich	$q_t = \frac{1}{\beta}\ln(\alpha\beta) + \frac{1}{\beta}\ln t$	α, β	62
Intraparticle diffusion	$q_t = k_{id}\sqrt{t} + l$	k_{id}, l	61

†q_t, quantity of adsorbate adsorbed at time t (mg g^{-1}); q_{eq}, quantity of adsorbate adsorbed at equilibrium (mg g^{-1}); α, adsorption rate constant (mg g^{-1} min^{-1}); β, desorption rate constant (g mg^{-1}); k_1, pseudo-first order rate constant (min^{-1}); k_2, pseudo-second order rate constant (g mg^{-1} min^{-1}); k_{id}, intraparticle diffusion rate constant (mg g^{-1} $min^{0.5}$); l, is a constant related to the boundary layer thickness (mg g^{-1}).

Table 3: Isotherm models investigated for the adsorption of RhB onto $CoFe_2O_4$, MWCNT-COOH, and CNT-$CoFe_2O_4$ composites

Isotherm model	Equation	Parameters†	References
Langmuir	$q_{eq} = \frac{q_m b C_{eq}}{1 + b C_{eq}}$	q_m, b	67
Freundlich	$q_{eq} = K_F C_{eq}^{1/n}$	K_F, n	66
Temkin	$q_{eq} = \frac{RT}{b_T} ln(A_T C_{eq})$	b_T, A_T	68
Dubinin-Radushkevich	$q_{eq} = q_m e^{-\beta\varepsilon^2}$ $\varepsilon = RTln\left(1 + \frac{1}{C_{eq}}\right)$	q_m, β	69
Sips	$q_{eq} = \frac{b q_m C_{eq}^{1/n}}{1 + b C_{eq}^{1/n}}$	q_m, b, n	70
Toth	$q_{eq} = \frac{q_m C_{eq}}{\left(\frac{1}{K_T} + C_{eq}^{n_T}\right)^{1/n_T}}$	q_m, K_T, n_T	73
Redlich-Peterson	$q_{eq} = \frac{K_{RP} C_{eq}}{1 + a_{RP} C_{eq}^{g}}$	K_{RP}, a_{RP}, g	72
Khan	$q_{eq} = \frac{q_m b_K C_{eq}}{\left(1 + b_K C_{eq}\right)^{a_K}}$	q_m, a_K, b_K	71

†q_{eq}, adsorption capacity (mg g^{-1}); C_{eq}, equilibrium concentration of adsorbate in solution (mg dm^{-3}); q_m, maximum monolayer capacity (mg g^{-1}); b, Langmuir isotherm constant (dm^3 mg^{-1}); K_F, Freundlich isotherm constant (mg g^{-1})(dm^3 $mg^{-1})^n$; n, adsorption intensity; b_T, Temkin isotherm constant; A_T, Temkin isotherm equilibrium binding constant (dm^3 g^{-1}); β, Dubinin-Radushkevich isotherm constant (mol^2 kJ^{-2}); K_t, Toth isotherm constant (mg g^{-1}); n_T, Toth isotherm constant; K_{RP}, Redlich-Peterson isotherm constant (dm^3 g^{-1}); a_{RP}, Redlich-Peterson

isotherm constant; g, Redlich-Peterson isotherm exponent; a_k, Khan isotherm exponent; b_k, Khan isotherm constant.

Table 4: Textural characteristics of adsorbents

Entry	Adsorbent	Surface area/m^2 g^{-1}	Pore volume/cm^3 g^{-1}	Pore diameter/nm	I_D/I_G	pH_{PZC}
1	$CoFe_2O_4$	116.4	0.158	4.568	-	7.00
2	Pristine-MWCNTs	108.8	0.494	18.44	1.17	-
3	MWCNT-COOH	126.8	0.692	22.95	1.19	4.02
4	29 %	128.1	0.400	10.98	0.22	6.20
5	50 %	140.0	0.544	14.87	0.35	6.16
6	75 %	293.4	1.160	16.89	0.83	4.50

Table 5: Kinetics parameters for adsorption of RhB [Conditions: 25cm^3 of 100 mg dm^{-3} or 50 mg dm^{-3} RhB for $CoFe_2O_4$, MWCNT-COOH, 29 %, 50 % and 75 % MWCNT-$CoFe_2O_4$ nanocomposites, pH 7.0, 50 mg of adsorbent, agitation speed 150 rpm, temperature 20 °C]

Model	Parameters	$CoFe_2O_4$	29 %	50 %	75 %	MWCNT-COOH
Experimental	q_{meas}/mg g^{-1}	5.673	19.40	21.08	32.49	49.19
Pseudo-first order	k_1/min^{-1}	-	-	-	0.014	0.017
	q_{eq}/mg g^{-1}	-	-	-	31.25	47.23
	RSE[a]	-	-	-	0.749	0.693
	SSR[b]	-	-	-	55.76	274.0
Pseudo-second order	k_2/g mg^{-1} min^{-1}	3.685	1.472	1.932	0.543	0.507
	q_{eq}/mg g^{-1}	5.877	19.43	20.86	34.61	51.26
	RSE	0.093	0.013	0.098	0.438	0.509
	SSR	0.453	6.870	14.28	25.63	146.2
Intraparticle diffusion	k_{id}/ mg g^{-1} min$^{-0.5}$	0.223	0.767	0.859	1.282	1.994
	I/mg g^{-1}	0.659	0.719	0.893	2.804	7.086
	RSE	1.447	1.355	1.452	1.654	1.662
	SSR	33.48	473.7	703.2	1076	3213
Elovich	α/mg g^{-1} min^{-1}	0.434	1.943	3.798	2.235	5.860
	β/g mg^{-1}	1.023	0.316	0.319	0.173	0.127
	RSE	0.287	0.926	1.038	1.432	2.033
	SSR	1.457	23.58	25.22	86.04	208.1

[a]RSE - residual standard error, [b]SSR - sum of squared residuals.

Table 6: Isotherm parameters for the adsorption of RhB onto $CoFe_2O_4$ and 29% composite

Adsorbent	Isotherm	Parameters	Temperature/K				Adsorbent	Temperature/K			
			293 K	303 K	313 K	318 K		293 K	303 K	313 K	318 K
$CoFe_2O_4$							29 %				
	Langmuir	q_m	5.165	5.289	6.102	7.950		21.17	20.24	21.32	20.60
		b	0.092	0.154	0.134	0.103		0.222	0.652	0.846	2.401
		RSE	0.738	0.909	1.004	0.746		1.464	0.849	1.116	0.923
		SSR[b]	0.053	0.454	0.642	3.602		10.71	3.608	6.230	5.111
	Freundlich	K_F	1.120	1.688	1.782	1.981		6.345	9.189	10.25	12.22
		n	3.080	3.753	3.512	3.207		3.126	4.220	4.341	5.868
		RSE	0.425	2.302	4.257	10.34		2.570	2.330	2.566	2.472
		SSR	0.278	0.122	0.436	4.462		33.03	27.15	32.93	36.65
	Temkin	b_T	2060	-	-	-		24.58	-	-	-
		A_T	1.605	-	-	-		836.9	-	-	-
		SSR	2.955	1.552	1.83	6.274		79.31	18.26	23.31	51.69
	D-R	q_m	4.909	-	-	-		17.12	-	-	-
		n	474.7	-	-	-		2005	-	-	-
		SSR	7.154	5.156	5.544	16.42		203.3	37.96	31.38	122.56
	Sips	q_m	17.87	19.61	20.85	20.16		17.87	19.61	20.85	20.16
		b	0.085	0.666	0.885	3.203		0.084	0.666	0.885	3.203
		n	0.500	0.876	0.909	0.797		0.499	0.876	0.909	0.797

	RSE	0.383	0.889	1.223	0.908	0.383	0.889	1.223	0.908
	SSR	1184	1414	1639	1679	0.586	3.163	5.987	4.119
Toth	q_m	0.299	0.2987	0.299	0.856	47.32	-	47.3	0.856
	K_T	-1.269	-1.269	-1.269	-0.888	23.94	-	23.94	-0.888
	n_T	0.604	0.60372	0.604	0.667	1.291	-	1.291	0.667
	SSR	0.084	-	4.920	0.305	7.236	75.22	156.4	-
R-P	K_{RP}	3.080	11.88	17.11	49.98	3.08	11.88	17.11	49.98
	α_{RP}	0.039	0.519	0.759	2.444	0.039	0.520	0.760	2.444
	g	1.382	1.039	1.019	0.997	1.382	1.039	1.019	0.997
	RSE	1.402	2.062	1.869	0.859	0.923	0.902	1.236	1.011
	SSR	1062	1395	1634	1715	3.408	3.251	6.115	5.106
Khan	q_m	48.60	23.27	23.27	33.00	48.60	23.27	23.27	33.00
	α_K	1.129	1.050	0.523	0.961	1.129	1.050	1.051	0.961
	b_K	0.272	0.523	1.051	2.238	1.213	0.902	0.523	3.032
	RSE	1.231	0.902	1.992	3.032	0.148	2.479	1.103	0.208
	SSR	5209	1390	1342	8267	1308	3.255	23.11	1510

[a]RSE - residual standard error, [b]SSR - sum of squared residuals.

Table 7: Isotherm parameters for the adsorption of RhB onto 50% and 75% nanocomposites

Adsorbent	Isotherm	Parameters	Temperature/K 293 K	303 K	313 K	318 K	Adsorbent	Temperature/K 293 K	303 K	313 K	318 K
50 %							75 %				
	Langmuir	q_m	21.79	24.13	23.90	24.63		35.91	37.67	37.51	38.10
		b	3.247	1.380	2.760	3.006		0.426	0.552	1.156	1.681
		RSE[a]	4.604	4.070	4.666	0.734		1.340	1.671	2.406	2.868
		SSR[b]	40.30	126.1	127.6	130.6		14.36	22.34	46.30	65.81
	Freundlich	K_F	14.69	15.93	17.59	18.38		13.46	15.40	18.91	22.24
		n	6.613	7.521	9.717	10.50		3.513	3.703	4.536	5.241
		RSE	4.474	4.167	4.899	0.388		3.945	4.736	5.769	3.890
		SSR	34.97	134.0	136.1	144.0		124.5	179.5	266.2	121.0
	Temkin	b_T	2060	-	-	-		2060	-	-	-
		A_T	1.605	-	-	-		1.605	-	-	-
		SSR	-	-	-	-		4643	5160	5752	-
	D-R	q_m	21.43	-	-	-		31.63	-	-	-
		β	3143	-	-	-		1782	-	-	-
		SSR	713.6	205.9	143.5	-		395.6	191.3	116.4	363.9
	Sips	q_m	27.27	19.61	20.85	20.16		34.64	36.51	35.14	40.77
		b	1.199	0.666	0.885	3.203		0.347	0.517	1.815	1.269
		n	2.128	0.876	0.909	0.797		0.847	0.803	0.595	1.463
		RSE	-	-	-	-		1.277	1.352	1.686	2.705
		SSR	153.6	487.1	-	-		40.15	13.40	13.50	69.74
	Toth	q_m	0.299	-	0.299	0.856		0.299	-	0.299	0.856
		K_T	-1.269	-	-1.269	-0.888		-1.269	-	-1.269	-0.888
		n_T	0.604	-	0.604	0.667		0.604	-	0.604	0.667
		SSR	-	-	-	-		-	-	-	-

R-P	K_{RP}	183.4	11.88	17.11	49.98	12.55	160.3	17.11	49.98
	α_{RP}	11.14	0.519	0.7595	2.444	0.258	0.288	0.760	2.444
	g	0.890	1.039	1.019	0.997	1.091	1.124	1.018	0.997
	RSE	-	-	-	-	1.206	1.277	1.236	1.011
	SSR	155.9	487.4	-	-	10.18	11.42	1526	1427
Khan	q_m	11.98	22.13	22.13	33.00	48.60	56.37	56.37	33.00
	a_K	0.885	0.985	3.155	0.961	1.129	1.175	1.175	0.961
	b_K	13.17	3.156	0.985	2.238	0.272	0.305	0.305	2.238
	RSE	-	-	-	-	1.213	1.313	1.659	3.032
	SSR	156.2	132.4	-	-	10.30	12.07	321.0	544.3

[a]RSE - residual standard error, [b]SSR - sum of squared residuals.

Table 8: Isotherm parameters for the adsorption of RhB onto MWCNT-COOH

			Temperature/K			
Adsorbent	**Isotherm**	**Parameters**	**293 K**	**303 K**	**313 K**	**318 K**
MWCNT-COOH	Langmuir	q_m	42.68	45.80	45.49	51.08
		b	0.794	1.070	5.000	4.137
		RSE[a]	0.779	1.975	2.025	3.632
		SSR[b]	4.860	31.21	32.79	105.5
	Freundlich	K_F	18.89	22.31	31.03	1.922
		n	3.525	3.531	4.891	3.183
		RSE	4.638	4.750	6.543	0.388
		SSR	172.1	180.5	342.5	269.3
	Temkin	b_T	2060	-	-	-
		A_T	1.605	-	-	-
		SSR	6547	7378	9377	-
	D-R	q_m	36.32	-	-	-
		β	3917	-	-	-
		SSR	1094	570.7	356.5	604.6
	Sips	q_m	41.63	47.24	45.40	20.16
		b	0.827	0.999	5.098	3.203
		n	0.920	1.098	0.992	0.797
		RSE	0.706	2.050	2.164	0.908
		SSR	3.487	29.41	32.77	4308
	Toth	q_m	0.299	-	306.8	0.856
		K_T	-1.269	-	1286	-0.888
		n_T	0.604	-	3.251	0.667
		SSR	-	-	128.6	-
	R-P	K_{RP}	29.91	11.88	17.11	154.2
		α_{RP}	0.606	0.520	0.760	2.471
		g	1.053	1.037	1.019	1.109
		RSE	0.578	0.902	1.236	2.955
		SSR	2.337	3105	4870	61.13
	Khan	q_m	51.58	51.59	51.59	33.00
		a_K	1.075	1.045	1.045	0.961
		b_K	0.596	0.885	0.885	2.238
		RSE	0.566	2.083	4.211	3.032
		SSR	2.240	30.37	1366	1998

[a]RSE - residual standard error, [b]SSR - sum of squared residuals.

Table 9: Summary of the best fit isotherm parameters for the adsorption of RhB onto $CoFe_2O_4$, MWCNT-COOH, 29 %, 50 % and 75 % MWCNT-$CoFe_2O_4$ nanocomposites

Adsorbent	Isotherm	Parameters	Temperature/K			
			293 K	303 K	313 K	318 K
$CoFe_2O_4$	Langmuir	q_m	5.165	5.289	6.102	7.950
		b	0.092	0.154	0.134	0.103
		RSE	4.604	4.070	4.666	0.734
		SSR[b]	0.053	0.454	0.642	3.602
	Freundlich	K_F	1.120	1.688	1.782	1.981
		n	3.080	3.753	3.512	3.207
		RSE	0.425	2.302	4.257	10.34
		SSR	0.278	0.122	0.436	4.462
29 %	Langmuir	q_m	21.17	20.24	21.32	20.60
		b	0.222	0.652	0.846	2.401
		RSE	1.464	0.849	1.116	0.923
		SSR	10.71	3.608	6.230	5.111
	Sips	q_m	17.87	19.61	20.85	20.16
		b	0.084	0.666	0.885	3.203
		n	0.499	0.876	0.909	0.797
		RSE	0.383	0.889	1.223	0.908
		SSR	0.586	3.163	5.987	4.119
50 %	Langmuir	q_m	21.79	24.13	23.90	24.63
		b	3.247	1.380	2.760	3.006
		RSE	4.604	4.070	4.666	0.734
		SSR	40.30	126.1	127.6	130.6
	Freundlich	K_F	14.69	15.93	17.59	18.38

		n	6.613	7.521	9.717	10.50
		RSE	4.474	4.167	4.899	0.388
		SSR	34.97	134.0	136.1	144.0
75 %	Langmuir	q_m	35.91	37.67	37.51	38.10
		b	0.426	0.552	1.156	1.681
		RSE	1.340	1.671	2.406	2.868
		SSR	14.36	22.34	46.30	65.81
	Sips	q_m	34.64	36.51	35.14	40.77
		b	0.347	0.517	1.815	1.269
		n	0.847	0.803	0.595	1.463
		RSE	1.277	1.352	1.686	2.705
		SSR	40.15	13.40	13.50	69.74
MWCNT-COOH	Langmuir	q_m	42.68	45.80	45.49	51.08
		b	0.794	1.070	5.000	4.137
		RSE	0.779	1.975	2.025	3.632
		SSR	4.86	31.21	32.79	105.5

[a]RSE - residual standard error, [b]SSR - sum of squared residuals.

Table 10: Thermodynamic parameters for the adsorption of RhB onto $CoFe_2O_4$, 29 %, 50 %, 75 % composites and MWCNT-COOH

Adsorbent	*T*/K	$\Delta G°$/kJ mol^{-1}	$\Delta H°$/kJ mol^{-1}	$\Delta S°$/J K^{-1} mol^{-1}
$CoFe_2O_4$	293	-15.01 ± 0.13		
	303	-16.88 ± 0.34		
	313	-17.45 ± 0.52	15.95 ± 0.01	106.7 ± 0.06
	318	-17.73 ± 0.11		
29 %	293	-20.60 ± 0.39		
	303	-23.90 ± 0.44		
	313	-25.50 ± 0.18	65.02 ± 0.33	292.3 ± 0.21
	318	-28.58 ± 0.13		
50 %	293	-27.21 ± 0.66		
	303	-25.42 ± 0.72		
	313	-27.04 ± 0.13	-5.581 ± 0.26	70.51 ± 0.11
	318	-29.19 ± 0.16		
75 %	293	-23.47 ± 0.43		
	303	-25.05 ± 0.47		
	313	-27.79 ± 0.33	44.87 ± 0.10	232.3 ± 0.24
	318	-29.26 ± 0.22		
MWCNT-COOH	293	-25.41 ± 0.16		
	303	-27.21 ± 0.71		
	313	-32.10 ± 0.64	65.17 ± 0.08	307.9 ± 0.02
	318	-32.42 ± 0.33		

Table 11: Comparison of adsorption capacities of various reported adsorbents for rhodamine B with present study

Adsorbents	Conditions	q_m/mg g^{-1}	References
Pristine MWCNT	pH 7.0, C_i 10 mg dm^{-3}, 10 min, 100 mg dose	3.533	[80]
Fe_3O_4/MWCNT-COOH	pH 6.0, C_i 15 mg dm^{-3}, 80 min, 3 mg dose, 298 K	11.44	[81]
Activated carbon	pH 2.3, C_i 40 mg dm^{-3}, 60 min, 8 mg dose, 313 K	4.93	[82]
Fe_3O_4-activated carbon	pH 4.0, C_i 20 mg dm^{-3}, 45 min, 30 mg dose, 298 K	47.62	[83]
Fe_3O_4/humic acid	pH 6.0, C_i 50 mg dm^{-3}, 15 min, 50 mg dose	161.8	[84]
$CoFe_2O_4$	pH 7,0, C_i 50 mg dm^{-3}, 360 min, 50 mg dose, 293 K	5.17	This Study
MWCNT-$CoFe_2O_4$ (29 %)	pH 7,0, C_i 50 mg dm^{-3}, 360 min, 50 mg dose, 293 K	21.17	This Study
MWCNT-$CoFe_2O_4$ (50 %)	pH 7,0, C_i 50 mg dm^{-3}, 360 min, 50 mg dose, 293 K	21.79	This Study
MWCNT-$CoFe_2O_4$ (75 %)	pH 7,0, C_i 100 mg l^{-1}, 360 min, 50 mg dose, 293 K	35.91	This Study
MWCNT-COOH	pH 7,0, C_i 100 mg dm^{-3}, 360 min, 50 mg dose, 293 K	42.68	This Study

Table 12: Percentage desorption of RhB by using acetone or ethanol [Conditions: 10 cm^3 of either acetone or ethanol, 50 mg of RhB-loaded adsorbent, agitation speed 150 rpm, equilibration time 30 min, and temperature 20 °C]

Adsorbents	Desorption/%	
	Acetone	Ethanol
$CoFe_2O_4$	90.60	88.61
29 %	93.20	64.23
50 %	82.46	62.45
75 %	80.41	74.50
MWCNT-COOH	94.63	82.52

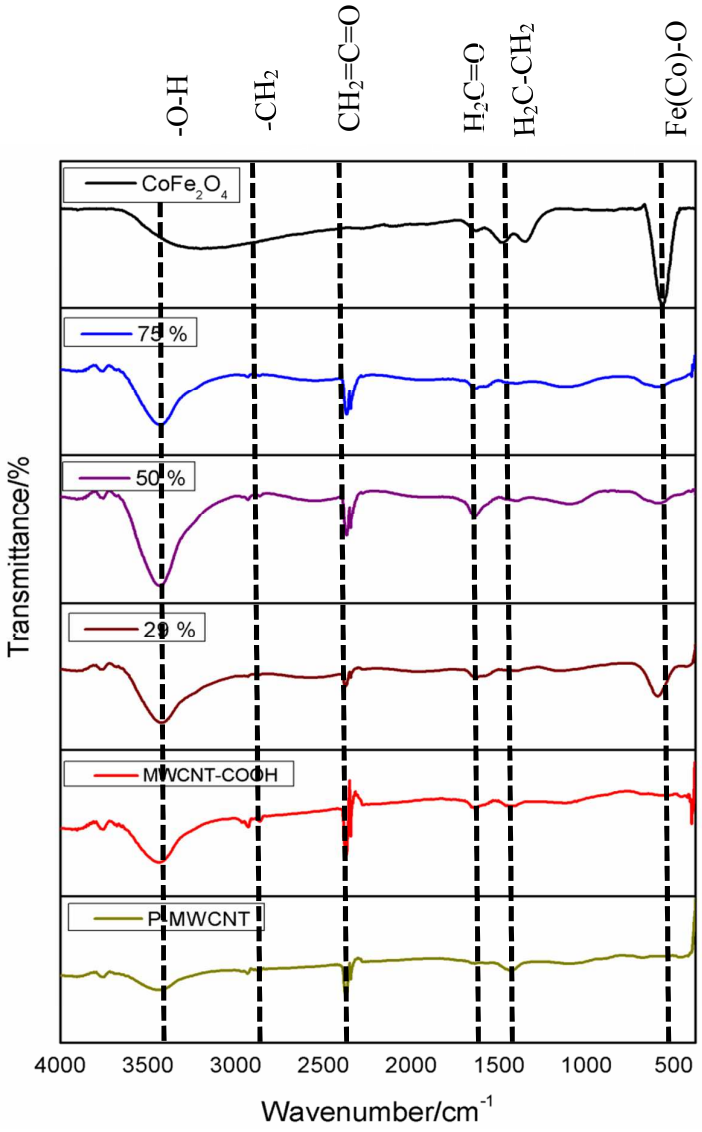

Fig. 1: FTIR spectra of pristine-MWCNT, MWCNT-COOH, $CoFe_2O_4$ and CNT-$CoFe_2O_4$ nanocomposites.

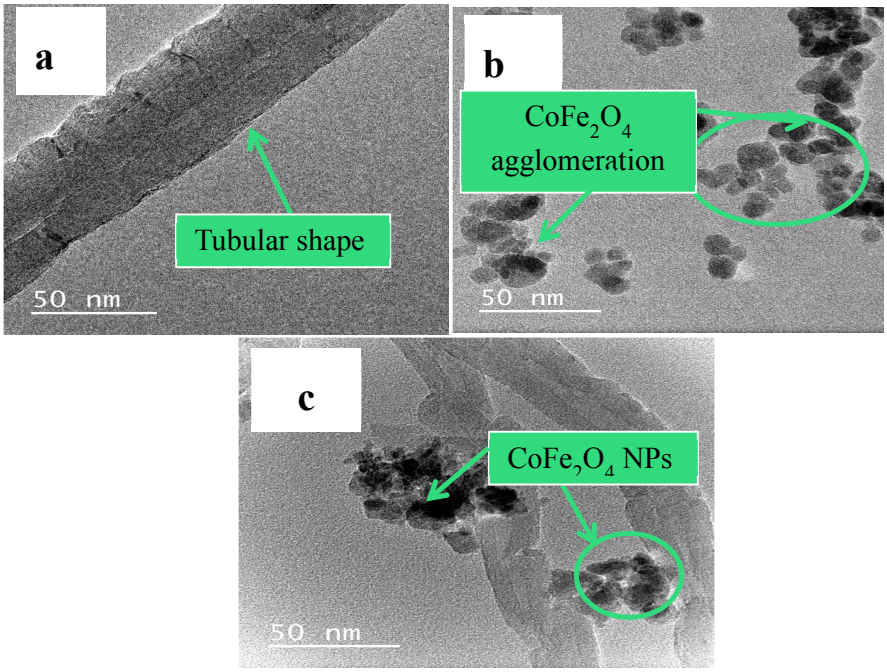

Fig. 2: HRTEM images of (a) MWCNT-COOH, (b) $CoFe_2O_4$ nanoparticles and (c) 29 % MWCNT-COOH-$CoFe_2O_4$ nanocomposites.

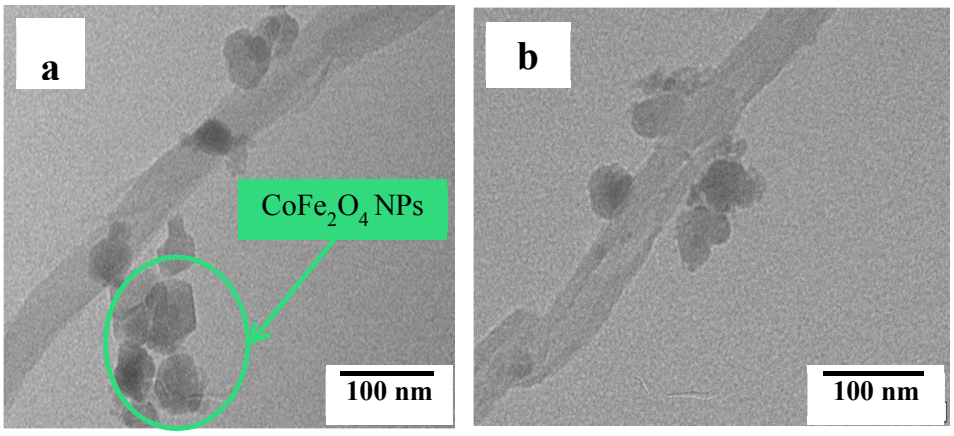

Fig. 3: TEM images of (a) 29 % and (b) 75 % MWCNT-COOH-$CoFe_2O_4$ nanocomposites.

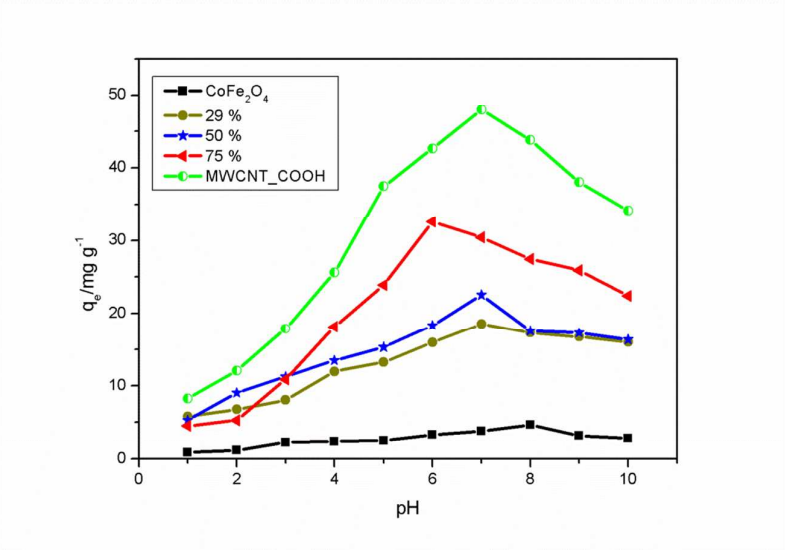

Fig. 4: Effect of pH on the adsorption of RhB [Conditions: 25 cm^3 of 100 mg dm^{-3} or 50 mg dm^{-3} RhB, 24 h equilibration time, 50 mg adsorbent dose, agitation speed 150 rpm, temperature 20 °C].

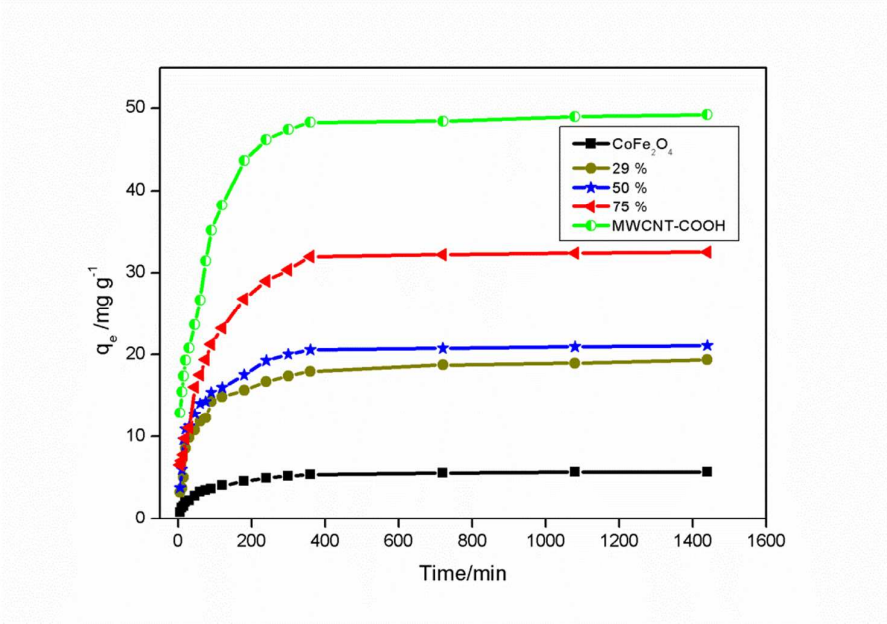

Fig. 5: Effect of contact time on the adsorption of RhB [Conditions: 25 cm^3 of 100 mg dm^{-3}or 50 mg dm^{-3} RhB, 50 mg adsorbent dose, pH 7, agitation speed 150 rpm, temperature 20 °C].

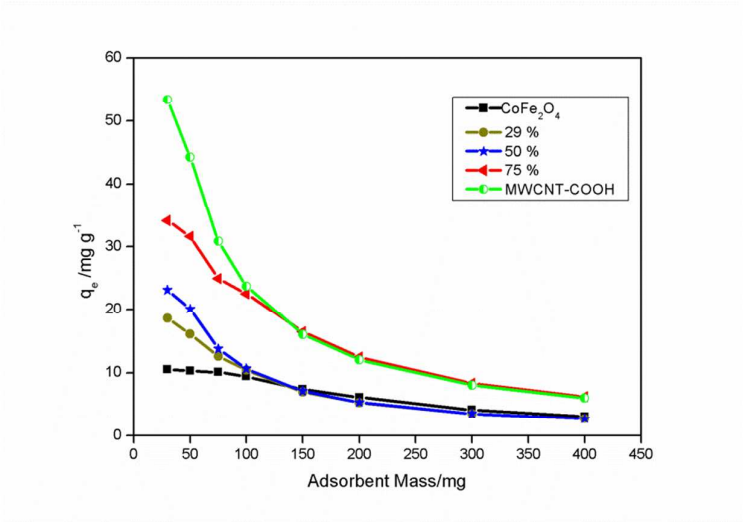

Fig. 6: Effect of adsorbent dose on the adsorption of RhB [Conditions: 25 cm^3 of 100 mg dm^{-3} or 50 mg dm^{-3} RhB, 24 h equilibration time, pH 7, agitation speed 150 rpm, temperature 20 °C].

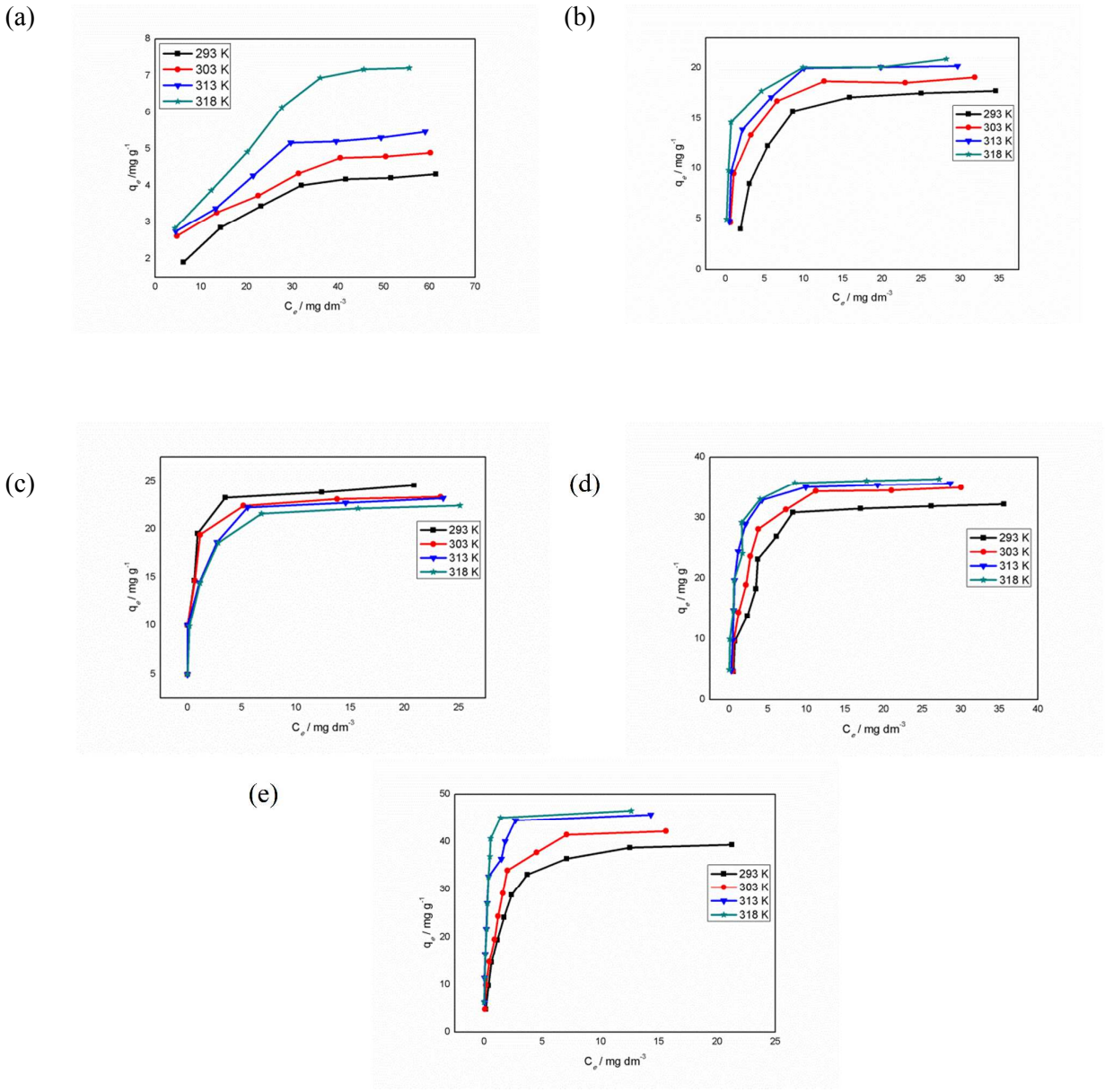

Fig 7: Effect of change in temperature on the adsorption of RhB (a) $CoFe_2O_4$, (b) 29 %, (c) 50 %, (d) 75 % MWCNT-COOH-$CoFe_2O_4$ nanocomposites and (e) MWCNT-COOH [Conditions: 25 cm^3 of 100 mg dm^{-3} or 50 mg dm^{-3} RhB, 24 h equilibration time, pH 7, agitation speed 150 rpm, 50 mg adsorbent dose].